S. Maeda, J. Kasahara, and A. Matsuo,
Combustion and Flame, Vol. 159 (2012) pp. 887-896.

1. Title：

Oblique Detonation Wave Stability Around a Spherical Projectile by a High Time Resolution Optical Observation

2. Authors and affiliations：

SHINICHI MAEDA[1], JIRO KASAHARA[1] AND AKIKO MATSUO[2]

[1]*Department of Engineering Mechanics and Energy*
University of Tsukuba
1-1-1 Tennodai, Tsukuba, 305-8573, Japan
[2]*Department of Mechanical Engineering*
Keio University
3-14-1 Hiyoshi, Kohoku-ku, Yokohama, 223-8522, Japan

3. Corresponding author's complete contact information：

Mailing address:
Jiro KASAHARA, Department of Engineering Mechanics and Energy
University of Tsukuba, 1-1-1 Tennodai, Tsukuba, 305-8573, Japan
Tel / Fax: 0011-81-29-853-5267
Email: kasahara@kz.tsukuba.ac.jp

S. Maeda, J. Kasahara, and A. Matsuo,
Combustion and Flame, Vol. 159 (2012) pp. 887-896.

Abstract

Spherical projectiles were launched into detonable mixtures over a wide range of projectile velocities from near to about 1.8 times the Chapman-Jouguet (C-J) velocity. Oblique detonation waves (ODWs) and shock-induced combustions (SICs) stabilized around the projectiles were visualized with high time and high spatial resolutions using the Schlieren technique and a high-speed camera with a 1-μs frame speed. Unsteady wave structures called Straw Hat type structures consisting of a SIC region followed by a C-J ODW were observed near stabilizing criticalities of a C-J ODW, and they were divided into two propagation types, depending on whether the C-J ODW could be stabilized (Kasahara *et al.* 2001, 2002, Maeda *et al.* 2011). In the present study, we suggested wave structures of the Straw Hat types based on our examination of dozens of continuous images. Triple points were observed at the intersection of a bow shock, a C-J ODW and a transverse detonation or shock wave when projectile velocities were slightly higher than C-J velocities. Onsets of local explosions in the SIC region for stabilizing the ODW in the Straw Hat type structures have been reported (Maeda *et al.* 2011). We observed this stabilizing mechanism by visualizing onsets of periodical local explosions and their transition to spherical detonation waves when the projectile velocity was much higher than the C-J velocity. We also determined stabilizing criticalities using a stoichiometric acetylene-oxygen mixture diluted with argon or krypton in 50% or 75% volumetric fractions, respectively. We found that the stabilizing criticalities did not depend only on the ratio of the projectile diameter and the cell size of the mixture.

S. Maeda, J. Kasahara, and A. Matsuo,
Combustion and Flame, Vol. 159 (2012) pp. 887-896.

Keywords

Hypersonic projectiles, Detonation initiation, Oblique detonation waves, High-speed camera

1. Introduction

An oblique detonation wave (ODW) occurs around a body in a hypersonic detonable mixture flow when the flow velocity is higher than the self-propagation velocity (Chapman-Jouguet (C-J) velocity) of a detonation wave. This also occurs when a projectile flies at hypersonic speed in a detonable mixture at rest. An oblique detonation wave engine (ODWE) (Powers [1]) and a ram-accelerator (RAMAC) (Hertzberg *et al.* [2], Higgins [3]) are two concepts that rely on a stabilized ODW in a combustor. To realize these engines, it will be necessary to understand the critical conditions and mechanism needed to initiate and stabilize an ODW. The experimental visualization of an ODW stabilized around a hypersonic projectile was first reported by Lehr [4]. Lee [5] and Vasiljev [6] proposed an analytical equation to estimate the energy required to initiate a detonation wave by a projectile. This equation was constructed using a simple cylindrical blast-wave theory excluding chemical reactions. Empirical values were specifically used for a critical blast radius and strength to calculate the critical energy. Higgins and Bruckner [7] compared their experimental results with the Lee and Vasiljev initiation criticalities [5, 6]. In the study by Higgins and Bruckner, spherical projectiles were launched into stoichiometric hydrogen-oxygen mixtures

diluted with argon in a 70% volumetric fraction. Projectile velocities ranged widely, from below to near the C-J velocity. Detailed ODW formation processes were not clear, because they confirmed initiations of ODWs only by using pressure recordings on a chamber wall without visualization. Kaneshige and Shepherd [8] launched spherical projectiles with a 25-mm diameter into stoichiometric hydrogen-oxygen mixtures diluted with nitrogen, and projectile velocities were near the C-J velocity. They compared characteristic time scales of a chemical reaction to that of a flow behind a local shock wave to discuss stabilization criticalities of an ODW around a projectile. Successes and failures of ODW stabilizations were confirmed using pressure recordings and visualizations. Verreault and Higgins [9] conducted visualizations of detonation initiations using cone-nosed cylinder projectiles while varying the cone half-angles from 15° to 60°. They discussed the wide-ranging dependences of the cone half-angles and mixture pressures on initiating criticalities using two requirements, the "energetic requirement" derived from Lee-Vasiljev's theory [5, 6] and the "chemical kinetic requirement" obtained by comparing the induction length on the cone surface (downstream of the shock attached to the cone tip) and the geometrical cone length. The projectile velocity was fixed at 1.5 times the C-J velocity. Therefore, the results didn't include dependences of projectile velocities on the phenomenon. These experimental studies [4, 7-9] have been conducted under limited projectile velocity conditions when the velocities were greater than the C-J velocity, and it has been difficult to assess the role of local phenomena, such as the curvature of the shock or

detonation waves, around the projectiles on the initiation and stabilization of an ODW.

Kasahara *et al.* [10-12] launched cone-nosed cylinders or spheres into detonable mixtures. In cone-nosed cylinder experiments [11], a wave structure of an ODW stabilized around a projectile was first proposed. In sphere experiments [12], projectile velocities were varied from near to 1.6 times the C-J velocity. Local curvature radiuses and shock or detonation propagation velocities near the projectiles were measured using Schlieren pictures, and stabilization criticalities of ODWs were proposed. These criticalities were expressed by two nondimensional quantities, the nondimensional projectile velocity, which was the ratio of a projectile velocity to the C-J velocity, and the nondimensional projectile diameter, which was the ratio of a projectile diameter to the cell width. The critical nondimensional diameters were experimentally determined to be about 5, which was also concluded by the experimental investigation of Higgins and Bruckner [7]. An empirical equation relating the critical nondimensional diameters with the nondimensional velocities was proposed. Furthermore, an unsteady propagation of an ODW was visualized at the vicinity of the stabilizing criticality. It consisted of a shock-induced combustion (SIC) region around a projectile followed by an ODW, and Kasahara *et al.* called it a “Straw Hat type” structure. Although Chernyavskii *et al.* [13] reported a similar unsteady propagation like the Straw Hat type, they did not describe it in detail. Kaneshige and Shepherd [8] visualized a local explosion downstream of a SIC region near a stabilizing criticality of an ODW and described it as an unsteady

deflagration-to-detonation transition (DDT) process. However, visualizations using a single-frame camera have not allowed detailed investigations of the temporal evolution of these unsteady phenomena. Maeda *et al.* [14] conducted visualizations of detailed time histories of ODW propagations using the Schlieren technique and a high-speed camera with a 1-μs frame speed. They observed a Straw Hat type and the flow structure involved local explosions at the intersection of a SIC region and a stabilized ODW. However, they didn't discuss the wave structure at an intersection of a bow shock and an ODW or the dependences of projectile velocities on these unsteady phenomena.

In this study, we visualized the phenomena with high time and high spatial resolutions using a high-speed camera under conditions with or without the stabilization of ODWs around spherical projectiles. The mixture filling pressures were varied by small increments, especially in the vicinities of stabilizing criticalities in which unsteady Straw Hat type structures could be observed. We proposed and confirmed wave structures of the Straw Hat type based on dozens of continuous images. Projectile velocities were varied from 1.1 to 1.8 times the C-J velocity, and we also investigated the dependences of the projectile velocities on stabilizing conditions and unsteady phenomena occurring near the criticalities. Stabilization of the ODW could be directly determined by observation of continuous images of the flowfield with detailed time histories. We used two different diluents to investigate whether the criticality expressed by the nondimensional projectile

diameter is universal.

2. Experimental Setup and Conditions

Hypersonic spherical projectiles were launched into detonable mixtures at rest in a filled chamber, and Schlieren visualizations were conducted using an HPV-1 high-speed camera (312 × 260 pixels spatial resolution, Shimadzu). The experimental setup [14] consisted of four devices, shown as (1) through (4) in Fig. 1, as follows: (1) a two-stage light-gas gun, (2) an observation chamber with glass windows for optical access filled with detonable mixtures between diaphragms 1 and 2, (3) a Schlieren system and a high-speed camera, and (4) an evacuation chamber to capture the projectiles and burned gases. The projectiles launched by the gas gun broke a very thin (12-μm thickness) Mylar diaphragm (diaphragm 1 in Fig. 1) and entered the detonable mixture. A diode laser and photodiode were placed 200 mm downstream of the observation chamber inlet, and they detected the passage of the projectile. The signal from the photodiode triggered the high-speed camera through a delay generator. The optical observation region was circular with a 90-mm diameter, and the center of this region was located 400 mm downstream of the chamber inlet. The projectile then broke a Mylar diaphragm of 100-μm thickness (diaphragm 2 in Fig. 1) after passing the observation region and was captured in the evacuation chamber with the burned gas. Spherical projectiles were chosen to eliminate the difficulty of launching straight projectiles (zero angle of attack), which is required for conical projectiles. The projectile had a 4.76-mm diameter and was made of polyethylene. In Kaheshige and Shepherd's experiments [8], the observation chamber had a square cross-section and

the sides were about 6 times greater than the projectile diameter. In their experiments, parts of observed ODWs were over-driven because of Mach reflections with the chamber wall, and the effects of the chamber wall on stabilizing ODWs were considerable. In the present study, we designed the chamber diameter to be considerably larger, 63 times larger than the projectile diameter [12, 14], to avoid the chamber wall influences on phenomena inside the observation region. The recording conditions of the high-speed camera were a 1-μs frame speed, a 250-ns exposure time and a maximum of 100 continuous recorded frames in all experiments.

Projectile velocities were always higher than the C-J velocity, and cell widths were several-fold smaller than projectile diameters, to achieve stabilized ODWs around the projectiles. Detonable mixtures were stoichiometric acetylene / oxygen mixtures ($2C_2H_2 + 5O_2$) diluted with argon ($2C_2H_2 + 5O_2 + 7Ar$) or krypton ($2C_2H_2 + 5O_2 + 21Kr$) in a 50% or 75% volumetric fraction to lower the C-J velocity of the mixture. The C-J velocity of the $2C_2H_2 + 5O_2 + 7Ar$ mixtures was about 1960 m/s. However, the $2C_2H_2 + 5O_2 + 21Kr$ mixtures were characterized by a substantially lower C-J velocity of about 1300 m/s, and this allowed nondimensional projectile velocities (ratios of a projectile velocity to the C-J velocity, V_p / D_{CJ}) to vary over a wide range (Table 1). The nondimensional velocities were classified in three categories as low, medium or high conditions. The mixture filling pressure was varied for each velocity condition to obtain the critical value for stabilizing ODWs. The filling temperature was room temperature in each case. Cell widths were needed to calculate

nondimensional projectile diameters (ratios of the projectile diameter and the cell width, d / λ). The experimental results of Desbordes and Desbordes *et al*. [15, 16] were used to evaluate the cell sizes at different pressures for the two mixtures. The data were accessed from the Detonation Database (Kaneshige and Shepherd [17]). Fitting equations for these cell sizes (λ [mm]) as an exponential of filling pressures (p_0 [kPa]) gives $\lambda = 61.52 \times p_0^{-1.117}$ for the $2C_2H_2 + 5O_2 + 7Ar$ mixture and $\lambda = 138.4 \times p_0^{-1.206}$ for the $2C_2H_2 + 5O_2 + 21Kr$ mixture, and the cell sizes were interpolated or extrapolated by these equations for each set of experimental conditions. The C-J velocity for each set of conditions was calculated using the chemical equilibrium computation software STANJAN (Reynolds[18]). Minimal differences of mixture compositions existed among the experiments, due to the mixing processes we used for the detonable mixtures. The mixture compositions were checked by gas chromatography (GC-8APT, Shimadzu). Errors of equivalent ratios and dilution ratios were within 8.4% and 4.5%, respectively. Projectile velocities were determined by time histories of projectile locations using observed continuous images. The projectile locations were situated almost linearly over time, and thus velocity deficits in the observation region were negligible. The large collection of continuous pictures could show many of the projectile locations with good accuracy, and systematic errors of the projectile velocities were within ± 0.65%.

3. Results of the low V_p / D_{CJ} conditions

In this section, we discuss the results of using mixtures diluted with argon or krypton under the low V_p / D_{CJ} conditions. The projectile velocity conditions were V_p / D_{CJ} = 1.03～1.28. Figure 2 shows snapshots of the observed movies. Figures 2 (a) through (d) are the results of using the argon-diluted mixture, and (e) through (h) are the results of using the krypton-diluted mixture. The filling pressures are decreased from the top to the bottom pictures in each case. These are negative pictures, and thus the white circles are the projectiles. The projectile travels from right to left. Similar trends were observed in both mixtures as the filling pressures decreased. These trends [12, 14] have been reported, and they were also observed using the different diluents in the present experiments. The stabilized ODWs shown in Figs. 2 (a) and (e) and the SICs shown in (d) and (h) were observed as almost steady phenomena with respect to the moving projectile. The nondimensional projectile velocities for the krypton-diluted mixture were about 10% lower than those of the argon-diluted mixture. This resulted in a slight difference in the C-J ODW angles in Figs. 2 (a) and (e). Regardless of the differences between V_p / D_{CJ} = 1.08 and V_p / D_{CJ} = 1.24 for the mixtures, the same tendency for the variable mixture filling pressures and almost the same wave structures were observed. Therefore, the differences in such a range would not have an influence on entire flowfields within the phenomena.

The studies of Maeda *et al.* [14] and Kasahara *et al.* [11] presented two types of Straw Hat type

structures near the critical conditions needed to stabilize ODWs; stabilized and attenuated ODW, respectively. These Straw Hat type structures exhibited a discontinuity between the SIC region and the ODW when the projectile velocities were just above the C-J velocity. However, unsteady shock-induced combustion phenomena occurred along the bow shock upstream of the transition point for the case of a stabilized ODW [14], whereas these unsteady phenomena decoupled from the bow shock upstream of the transition point for the case of an attenuated ODW [11]. Therefore, we call these two Straw Hat type structures the "Straw Hat type with a stabilized ODW" and the "Straw Hat type with an attenuated ODW". The detailed structure of these two types of flowfield has not yet been described, and we propose a description of these structures below.

Onsets of local explosions on shock-induced combustion phenomena have been reported [14] near the connection point between the bow shock and the ODW in Straw Hat types with stabilized ODWs. Therefore, bow-shocks and ODWs near the connection point are unsteady. The fundamental wave structure is given in Fig. 3, which shows a central cross section of the axisymmetric phenomenon. Because the bow shock coupled with unsteady SIC phenomena is connected to the conical ODW, the connection point (called the "transition point" in Fig. 3) between them has a triple point structure. Incident shock waves propagate from the transition point to a symmetrical line in a burned gas, and they probably make a Mach intersection near the symmetrical line.

Figures 2 (b) and (f) show snapshots of the movies in which Straw Hat types with stabilized

ODWs were observed for the argon- or krypton-diluted mixtures, respectively. The krypton-diluted mixtures had comparatively higher density than that of the argon-diluted mixtures, and therefore the tests with the krypton-diluted mixture (Fig. 2 (f)) allowed the imaging to have comparatively high contrast, and we can see the similar wave structure in Fig. 3. This wave structure could be seen in about 50 continuous pictures. The continuous pictures of Fig. 2 (f) are superposed with 4-μs intervals in Fig. 4. The bow shock and the unsteady SIC were coupled until reaching the transition point, and they were connected to the ODW. Because of the onsets of the local explosions, the wave fronts of the bow shock and the conical ODW were highly unsteady near the transition point. But the ODW propagating away from the projectile was steady, and therefore, it maintained a C-J propagation. Regarding Straw Hat types with stabilized ODWs for the argon-diluted mixture, Maeda *et al.* [14] reported that the C-J ODW was stabilized by the onsets of local explosions near the transition point, generating new ODW fronts. In Fig. 4, you can see that the distances between the trajectories of the transition points and the projectile at later times become smaller than those at earlier times, and new ODW fronts were generated. Therefore, the propagation type similar to the Straw Hat type with a stabilized ODW is also found in the krypton-diluted mixture.

The early computational work of Li *et al*. [19] showed the definite basic structure of a wedge-supported ODW behind an oblique shock. The configuration consisted in a hydrogen-oxygen-nitrogen mixture flowing at hypersonic velocities (1.5 to 1.8 times the C-J Mach

number) around a two-dimensional wedge of infinite length, and a non-reactive shock wave was basically attached to the wedge front. Energy release took place after an induction zone behind the non-reactive shock, and a set of deflagration waves was generated. These deflagration waves gradually converged into the initial non-reactive shock, and the ODW was initiated where the shock and the converged deflagration waves were coupled as a kink of the wave angles between the original shock and ODW. Although the flowfield resembled the Straw Hat type with stabilized ODW with respect to the transition from the SIC phenomenon to the ODW, this configuration has two important differences with experiments. One difference is that the shock wave is detached from the blunt-nosed projectile in our configurations. The strongest shock wave (the shortest induction zone) exists at the nose of the projectile, unlike the wedge case, in which the induction zone becomes shorter downstream of the non-reactive shock. And combustion instability [4, 10] is a feature of shock-induced combustion of a detached shock, as characterized by wave interaction between the detached shock and the projectile. In some cases, such instability locally initiates a detonation wave in a shock-induced combustion [20], and this may contribute to the initiation and stabilization of the ODW in the case of a Straw Hat type structure. Another difference is that the projectile has a finite length and three-dimensional geometry in our configurations. In the infinite wedge-supported ODW, there is no attenuating effect on the shock wave or detonation wave. On the other hand, they are attenuated by a rarefaction wave from the finite length projectile [11].

Additionally, the wave around the projectile is a three-dimensional conical wave. Therefore, a curvature effect on the wave exists by two curvature radiuses along or perpendicular to the wave [12]. The described differences of these features from those of the wedge-supported ODW will be also required for complete understanding of the complicated stabilization mechanism of the ODW in the Straw Hat type structure.

A wave structure of the Straw Hat type with an attenuated ODW is given in Fig. 5, which shows a central cross section of the axisymmetric phenomenon. Because the bow shock partially decoupled with the unsteady SIC is connected to the conical ODW, the transition point between them has a triple point structure. A shock-compressed unburned mixture exists at the decoupled region between the bow shock and the unsteady SIC. A transverse detonation wave or shock wave propagated from the transition point to a symmetrical line in the shock-compressed unburned mixture. Because the projectiles were hypersonic, between Mach 6.6 and 8.2, the shock wave angle should be smaller than 70° if the flow behind the shock wave is supersonic, based on two-dimensional oblique shock solutions under such upstream conditions. In addition, these phenomena are axisymmetric in reality, and thus the shock-compressions are weaker than those in the two-dimensional cases because of three-dimensional effects. However, we could not determine whether the flow Mach number behind the oblique shock upstream of the transition point was greater than the C-J Mach number in the shock-compressed unburned mixture. This transverse detonation wave or shock wave is connected to

the incident shock propagating in the burned gas generated in the SIC region, and the incident shock makes the Mach intersection near the symmetrical line.

Figures 2 (c) and (g) show snapshots of the movies in which Straw Hat types with attenuated ODWs were observed for the argon- or krypton-diluted mixtures, respectively. Only a few kilopascals difference in the filling pressures divided the Straw Hat type with a stabilized ODW from that with an attenuated ODW. The result of the krypton-diluted mixture (Fig. 2 (g)), which had comparatively higher density than that of the argon-diluted mixture, allowed the imaging to have comparatively high contrast, and we can see the similar wave structure in Fig. 5. This wave structure could be seen in about 50 continuous pictures. The continuous pictures of Fig. 2 (c) are superposed with 3-μs intervals in Fig. 6. The bow shock and unsteady SIC phenomena are decoupled at the transition point and are connected to the ODW without the local explosions. Therefore, the wave fronts of the bow shock and the conical ODW were steady near the transition point, unlike the Straw Hat type with a stabilized ODW. The ODW region is steady, and therefore, it maintains a C-J propagation. However, you can see that the trajectory of the transition points moves away from the trajectory of the projectile over time, as shown in Fig. 6. This means that the C-J ODW of the projectile trajectory side gradually disappeared over time.

Kasahara *et al.* [11] visualized the initiation process of a Straw Hat type with an attenuated ODW by conducting multipoint observations just after a diaphragm rupture by a projectile in separate

experiments. Their results revealed that the diaphragm rupture was responsible for the detonation initiation, and thus the C-J ODW was gradually attenuated over time below a stabilizing criticality. Therefore, we believe that the occurrence of the Straw Hat type with an attenuated ODW was to the result of the entrance phenomena at the chamber inlet (such as the diaphragm rupture and possibly a muzzle jet from a launch tube). A shock-induced combustion in both Straw Hat type structures has a column of reacted gases. Behrens *et al*. [21] have suggested that the gases inside the column were partly reacted gases and that a detonation wave propagated inside this gas column in some cases. We couldn't decide from our results whether a detonation wave existed in the gas column. Because we used the Schlieren method for visualizations, we could confirm a shock wave existing inside the gas column, but we couldn't confirm a chemical reaction behind the shock wave. Therefore, we labeled the wave inside the gas column as a shock wave in Figs. 3 and 5.

The propagation modes of these two Straw Hat type structures can be discussed by looking at the differences in the C-J ODW's wave angles. Figure 7 shows a relationship between the C-J ODW's wave angles measured from Schlieren images and the nondimensional projectile velocities. All experimental results, from low to high V_p / D_{CJ} conditions, are shown in this figure. The solid line in this figure denotes theoretical C-J angles calculated by the following equation: $\theta_{CJ} = \sin^{-1} (D_{CJ} / V_p)$, which is derived by a balance between projectile velocities and C-J velocities. The large error bars of one data point (V_p / D_{CJ} = 1.28, Detonation wave angle = 68°) are caused by the fact that the

observed ODW regions were small. Fully stabilized ODWs and Straw Hat types with stabilized ODWs indicated by closed and opened circles, respectively, present almost the same trends as the theoretical C-J angles. These results indicate that C-J ODWs are supported by the projectile velocities under these conditions. However, the Straw Hat types with attenuated ODWs indicated by triangles tend to have larger ODW angles than C-J angles. This means that horizontal propagation velocities of C-J ODWs are lower than the projectile velocities. The horizontal propagation velocities of the transition points, V_{tr}, were directly measured from the continuous pictures, and the results are listed in Table 2. Closed triangles in Fig. 7 show the relations between the measured V_{tr} / D_{CJ} and the measured C-J angles, and they agreed with the theoretical C-J angle relation. The V_{tr} are always lower than the projectile velocities, V_p, in both mixtures. However, the V_{tr} have almost the same values between the two different nondimensional projectile velocities in the argon-diluted mixture, which differed from those of the krypton-diluted mixture. The smaller V_{tr} than the V_p means that the relative distance between the projectile and the transition point becomes larger over time. As a result, the transition points trajectory moves away from the projectile trajectory along the bow shock, and the C-J ODW gradually disappears over time, as shown in Fig. 6. The SIC region of the Straw Hat type with an attenuated ODW observed in the argon-diluted mixture (Fig. 2 (c)) is longer than that of the krypton-diluted mixture (Fig. 2 (g)). The result with the argon-diluted mixture had a 15% higher nondimensional projectile velocity, and thus a longer SIC region (smaller ODW region)

was observed, since the distance between the chamber inlet and the observation region was fixed.

The critical conditions for stabilizing the ODW will be discussed collectively later in this paper.

4. Results of the medium and high V_p / D_{CJ} conditions

The medium and high nondimensional projectile velocities were achieved using only the krypton-diluted mixture, with V_p / D_{CJ} = 1.48～1.56 for the medium V_p / D_{CJ} conditions and V_p / D_{CJ} = 1.64～1.79 for the high V_p / D_{CJ} conditions. Snapshots of the observed movies are shown in Fig. 8. The results of the medium V_p / D_{CJ} conditions are shown in Figs. 8 (a) though (c) and (c'), and those of the high V_p / D_{CJ} conditions are shown in (d) and (e). Filling pressures go from higher to lower from the top to the bottom pictures in each column. The ODW angles plotted in Fig. 7 show the angles when the stabilized C-J ODWs were observed.

The Straw Hat type with a stabilized ODW under high V_p / D_{CJ} conditions near the stabilizing criticalities exhibited a different wave structure compared to the cases of low V_p / D_{CJ} conditions. As the projectile velocity increases, the ODW angle decreases and becomes comparable to the angle of the bow shock at the transition point. Therefore, the transition between the SIC region and the ODW is more continuous, and the triple point structure is no longer observed. The suggested wave structure under such conditions is shown in Fig. 9. The propagation velocity (wave angle) of the bow wave near the projectile decayed below the C-J velocity (C-J angle) and is accelerated to the C-J velocity (C-J angle) by unsteady local explosions. A variation of propagation velocities along the bow wave from near the projectile to the C-J ODW is expected to become gradual rather than discontinuous, as it is the case for the Straw Hat type with a stabilized ODW under the low V_p / D_{CJ}

conditions. Although the bow wave near the projectile and the ODW away from it are almost steady, unsteady wave motions are visible between them in Figs. 8 (b) and (e). This propagation mode is described as a stabilized ODW with an unsteady region in the figure. The continuous pictures of Fig. 8 (b) are superposed with 3-μs intervals in Fig. 10 as an example. A similar unsteadiness can be seen in Fig. 8 (e). Meanwhile, waves were almost steady in the whole region from near the projectile to the C-J ODW away from it in Figs. 8 (a) and (d).

More or less, the propagation velocity (wave angle) distribution along the wave had the point slightly below the C-J velocity (the C-J angle) near the projectile in all stabilized ODW cases (with and without an unsteady region) in Figs. 2 and 8. In this study, the stabilized ODWs were inherently three-dimensional conical waves. Therefore, a wave curvature effect on the wave would not be negligible near the projectile, where the wave curvature radius was relatively small. The propagation velocity (wave angle) of the bow wave near the projectile was decreased by the wave curvature effect. The curvature effect is more evident when the ratio of the wave curvature radius to a cell size (an induction length) is relatively small. Because the case in Fig. 8 (b) had a relatively low mixture filling pressure (that is, large cell size), being close to the stabilizing criticality of the conical ODW, the curvature effect on the ODW was more evident. In such a near critical condition, the detonation wave near the projectile would be close to a quenching limit by the curvature effect, which probably caused the instability on the wave front.

Another feature of the flowfield in the visualization results is the presence of belt-shaped luminescence regions behind the projectiles in Figs. 2 and 8. These regions are black in these figures because of the negative pictures. These may be wake regions of the projectile, and they are much clearer in the case of high projectile Mach number conditions such those shown in Fig. 8. A significantly high-temperature gas exists behind a shock wave near a stagnation point of the projectile. The gas flows downstream and forms the wake region, which emits a much stronger luminescence than the ODW does. This wake region is clearly visible farther downstream from the projectile, because it is surrounded by high-temperature burned gases, and the gas temperature in the wake region might not be rapidly decreased.

When the filling pressures were a few kilopascals lower than that of a stabilized ODW with an unsteady region, a Straw Hat type with an attenuated ODW is expected to occur and the SIC region should become much longer at high nondimensional projectile velocities, as discussed in the preceding section. The wave structure would be similar to that shown in Fig. 5. Although the ODW region was not observed together with the projectile in Fig. 8 (c), a part of the ODW region was observed in Fig. 8 (c') taken 46 μs after Fig. 8 (c). There are parts of the bow shocks at the top of the picture, and boundaries of the combustion waves are visible near the center, although they are unclear because of light saturation. It is very likely that a detonation wave was formed in the area shown at the right side of the picture, because striped patterns are visible behind this wave front.

This detonation wave is probably a wave front of the ODW region in the Straw Hat type with an attenuated ODW, as seen in Figs. 2 (c) and (g). The SIC region becomes much longer at these high nondimensional velocities, because differences between the projectile velocities and the horizontal propagation velocities of the ODW regions become larger under these conditions.

The effects of these velocity differences become more remarkable under the high V_p / D_{CJ} conditions. ODWs couldn't be observed within visualization times at either d / λ = 5.01 or d / λ = 5.89 under the high V_p / D_{CJ} conditions listed in Table 1. However, chamber wall pressures were recorded during these two experiments. Time histories of projectile locations and the chamber wall pressures in these cases are shown in Fig. 11. A pressure transducer was located at the center of the observation chamber, and this location corresponded to the zero-point of the projectile location in the figure. The zero-time corresponds to the time when the projectile passes in front of the diode laser. It is difficult to quantitatively discuss the pressure results, because the sensor head of the transducer was not uniformly placed with respect to the chamber wall; it was receding from the wall. However, it is possible to estimate whether detonation waves were initiated by looking for the presence of pressure peaks. The pressure peaks didn't exist after the projectile passed, in the results when d / λ = 5.01. Similar results were obtained when the projectiles were launched into inert (argon) gases with almost the same projectile Mach numbers. The waves were only bow shocks around the projectiles in the inert gases, and therefore, it is possible to expect that only a bow wave, that is, the SIC, was

present when $d / \lambda = 5.01$. The time when the bow shock reached the pressure transducer was long after the time range shown in Fig. 11, because the projectile velocity was hypersonic and the chamber diameter was much larger than the projectile diameter. The pressure peak existed about 800-μs after the projectile arrivals when the detonation wave was not initiated, including the case when the chamber was filled with inert gas (argon), but we couldn't decide whether the pressure peaks were to the result of the muzzle jet or the bow shock. However, the pressure peak was observed about 190 μs after the projectile passed when $d / \lambda = 5.89$. These apparent differences in the chamber wall pressures may indicate whether detonation waves were initiated. Therefore, the Straw Hat type with an attenuated ODW was present and the detonation waves existed far downstream of the SIC region under the high V_p / D_{CJ} conditions.

Finally, almost spherically expanding detonation waves were observed downstream of the SIC region near the stabilizing criticality of an ODW. Continuous pictures are shown with 5-μs intervals in Fig. 12. Times after the start of recording by the high-speed camera are shown in the upper left corner of each picture. In each of the pictures, the projectile location is fixed. The projectile locations after passing through the observation region are extrapolated by linear approximations and illustrated by open circles. A local explosion can be seen in the SIC region in the top picture (indicated by a black arrow). Farther downstream from this local explosion, striped patterns that are peculiar to detonation waves are visible behind the waves, which spread almost spherically. These spherical

detonations were probably initiated by local explosions that occurred outside of the observation region. The distance between the projectile and these detonation waves increases, because the projectile velocity was 1.8 times higher than the C-J velocity. Radulescu *et al.* [22] observed a similar phenomenon in quasi-cylindrical direct initiation experiments using line-shape explosive sources called "detonation cords." Similar to what occurred in our experiments, this phenomenon occurred under a critical condition (what they called a "critical regime") to initiate a steady ODW. Detonation velocities of the explosives in the detonation cords were significantly high, about 3 to 4 times higher than C-J velocities of ambient detonable mixtures, which were much higher than that of our experiments (up to 1.8 times the C-J velocity). The number of explosions (called "detonation bubbles") was decreased when the equivalence ratio of the ambient mixture was decreased from 1.0 to 0.98 remaining the initiation energy. The conical detonation was not obtained when the density of these explosions was insufficient. Interferences between these bubbles appeared to play a role in the transition into steady conical detonation waves. In this study, we couldn't observe this type of transition at the far field because of the limited area of visualization; however, this result indicates that the similar transition can occur in the hypersonic projectile initiation when the nondimensional projectile velocity is about 1.8. The sustaining mechanism of the C-J ODW in the Straw Hat type with a stabilized ODW, that is, the onsets of local explosions on shock-induced combustion phenomena, is made much clearer by this visualization result.

In some cases, especially in the krypton-diluted mixture, which had a relatively high density, we observed slight deceleration of the projectile (about 4% velocity reduction within the field-of-view) caused by drag forces in the observation region. However, even though quantitative determination of the drag force was impossible because of systematic errors resulting from spatial resolutions of the visualizations, there was no doubt that the projectiles decelerated in the detonable mixture. Therefore, if we have a very long observation region and can observe temporal processes of the phenomenon from the chamber inlet, the phenomenon observed in the high V_p / D_{CJ} conditions will be shifted to that of the medium and low V_p / D_{CJ} conditions as the projectile velocity decelerates. On the other hand, if the projectile velocity keeps constant, the wave structure is sustained for the given projectile velocity even in the case of a Straw Hat type with a stabilized ODW. In the Straw Hat type with an attenuated ODW, the entire wave structure shown in Fig. 5 will be sustained, but the ODW will gradually delay to the projectile over time. If the chamber has a finite cross-section diameter, the ODW will ultimately disappear and only the bow shock will exist.

5. Criticalities for stabilized C-J oblique detonation waves

In this section, we discuss stabilizing criticalities of ODWs around spherical projectiles using the results shown in previous sections. The observed phenomena in the various nondimensional projectile velocities and the filling pressures are plotted in Fig. 13. The "stabilized ODW with an unsteady region" observed under the medium and high V_p / D_{CJ} conditions is treated as the "stabilized ODW" regime. Critical filling pressures are found between the circle and triangle symbols in this figure. However, the critical filling pressure is about 71 kPa for the krypton-diluted mixture, and this pressure is less than half for the argon-diluted mixture, about 30 kPa. The filling pressures in Fig. 13 are converted into the nondimensional projectile diameters in Fig. 14, which shows the results for the argon- and krypton-diluted mixtures. The projectile diameters were constant in these experiments; therefore, only the cell widths were substantially varied. With respect to the results using the krypton-diluted mixture in Fig. 14, the results of Kasahara *et al.* [12], who used the same mixture, are plotted according to the experimental conditions given in their report. The solid line in Fig. 14 represents the following empirical equation:

$$(d / \lambda) = 4.97\, C_D^{-0.5} + 0.30\, (V_p / D_{CJ} - 1),$$

which represents the stabilizing criticality of an ODW around a spherical projectile suggested by Kasahara *et al.* [12]. In the equation, C_D denotes a drag coefficient of a projectile and is assumed to be $C_D = 1$ based on hypersonic Newtonian theory. In Fig. 14, we didn't include the Lee-Vasiljev's

criticality mentioned in the introduction, which shows the criticality for the "detonation stabilization" around a projectile, because we consider that the Lee-Vasiljev's theory means the criticality for the "detonation initiation" based on an energetic consideration by a projectile. Of course the Lee-Vasiljev's criticality should be the requirement for the stabilizing criticality, but the local condition on the wave is also needed to sustain the conical ODW when the projectile velocity is higher than the C-J velocity.

From Fig. 14, you can see that the stabilizing criticalities expressed by the nondimensional diameters are about 3.5 and 6.0 for the argon- and krypton-diluted mixtures, respectively, and they are different even in the same nondimensional velocity region. Figure 14 indicates that the critical nondimensional projectile diameter remains constant or increases slightly as the nondimensional velocity increases, and these results are consistent with those of Kasahara *et al.* Here, the visualization results are examined again to discuss the difference of the criticalities between the argon- and krypton-diluted mixtures. Cell structures are considered to be responsible for the striped patterns behind detonation waves, and therefore, we obtained the intervals between these patterns in the observed pictures. However, these are rough estimations, because the spatial resolutions of the pictures were not good enough to allow for a precise measurement. The chosen results for the estimations are Straw Hat types with stabilized ODWs (Figs. 2 (b) and (f)) under the low V_p / D_{CJ} conditions, because their cell widths are fairly close to those of the stabilization criticalities. The

intervals are between 1.1 mm and 1.6 mm for the argon-diluted mixture and 0.8 mm and 1.0 mm for the krypton-diluted mixture, and these are consistent with the cell widths of 1.3 mm and 0.8 mm, respectively, calculated from the fitting equations for the filling pressures and the cell widths. Note that we did not intend by these estimations to make direct measurements of the cell sizes from the Schlieren visualizations, because the pictures were results of an integration of the three-dimensional flowfield. Additionally, we couldn't decide what in cellular structures appeared as the striped patterns in the pictures. Therefore, these estimations lend themselves only to a qualitative assessment that a smaller cell size was needed to stabilize the C-J ODW in the krypton-diluted mixture than that of the argon-diluted mixture.

If detonable mixtures are highly diluted with monatomic inert gases (e.g., helium, argon and krypton) at volumetric fractions over 75%, transverse waves in multi-headed detonations are weakened and their cellular patterns have high regularity. This characteristic is considered to affect critical tube diameters for detonation propagations into unconfined spaces and critical energies for direct initiations of detonation waves. These critical values have been experimentally revealed to become higher than the cases when the mixtures were not diluted or were diluted at lower volumetric fractions (Desbordes [15], Lee [23]). The stabilizations of the ODWs should also depend on the characteristics of the chemical reaction behind a shock wave, and thus the differences of diluents and dilution ratios between these two mixtures should affect the stabilizing criticality of the ODW.

Higgins and Bruckner [7] have shown that the critical nondimensional projectile diameter was about 5 when the sphere diameter was varied from 6.35 mm to 19.1 mm while maintaining the mixture composition ($2H_2$+O_2+7Ar) and projectile velocity (equal to the C-J velocity), and these results agreed with the Lee-Vasiljev's theory [5, 6]. Kasahara *et al*. [12] have also shown almost the same criticality using a $2C_2H_2$+$5O_2$+21Kr mixture for a spherical projectile. Our experimental results indicate that the nondimensional projectile diameter of 5 was not a universal criticality that would be valid for any mixture composition. There is the possibility that we will need another parameter representing a mixture property in addition to the projectile diameter and the cell size to express the universal criticality for a sphere projectile subjected to different mixture compositions.

In this study, the stabilizing criticality of an ODW was expressed by global parameters; the projectile diameter and mixture cell size. To understand the underlying physics of this criticality, one should consider the local characteristics of a wave such as its velocity and curvature radius. These characteristics will determine the condition of a local point on the wave, and the criticality expressed by the global parameters will be a consequence of the criticality on the local point needed for sustaining a conical ODW. If a conical C-J ODW is steadily stabilized (as in Fig. 2 (a), (e) and Fig. 8 (a), (b), (d), (e)), the curvature effect on the detonation wave will not be negligible near the projectile where the curvature radius is small. If a mixture filling pressure is high enough (the cell size is small enough), the curvature effect is limited and the conical ODW will be sustained, and it will be

smoothly connected to a bow-shape detonation wave around the projectile. As the filling pressure is decreased, the conical ODW around the projectile will finally meet a quenching limit of a curved detonation, and the stabilizing will fail. On the other hand, an unsteady ODW stabilization in the Straw Hat type with a stabilized ODW cannot be explained by this type of curved detonation, because a bow wave around a projectile is no longer a detonation wave but rather is a bow shock and an unsteady shock-induced combustion phenomenon, as shown in Section 3. Mechanisms of the unsteady ODW stabilization in the Straw Hat type structure will be highly complicated compared to the steadily stabilized ODW cases, and we will also need to take into account the unsteady shock-induced combustion phenomena. When the mixture filling pressure is further decreased, a conical ODW is no longer sustained and a bow shock around the projectile finally decays to a Mach wave. With boundary conditions on experiments (such as a diaphragm rupture effect or muzzle jet effect), an ODW is initiated just below the stabilizing criticality to form the Straw Hat type with an attenuated ODW.

6. Conclusions

Hypersonic projectiles were fired into detonable mixtures while varying filling pressures near stabilizing criticalities of an ODW. The projectile velocities were also varied over a wide range, and Schlieren visualizations with high time and high spatial resolutions were conducted. Our tests revealed the wave structures of Straw Hat types with stabilized ODWs and Straw Hat types with attenuated ODWs near the stabilizing criticality. They had a triple point structure, where the SIC region was connected to the ODW region when the projectile velocity was slightly higher than the C-J velocity. We called these points "transition points."

In the Straw Hat type with a stabilized ODW, the wave structure consisted of a bow shock, a C-J ODW and an incident shock that propagated in the burned gas and made the Mach intersection. The triple point structure didn't appear when the projectile velocity was much higher than the C-J velocity, because the C-J angle of the ODW became smaller. The variation of the propagation velocities (wave angles) along the wave from the bow wave to the C-J ODW became gradual, unlike the lower projectile velocity cases. We also confirmed the onsets of local explosions to stabilize the ODW in the Straw Hat type structure by observing the spherical detonation waves initiated by the periodical local explosions on the SIC region when the nondimensional projectile velocity was 1.79. On the other hand, the wave structure of the Straw Hat type with an attenuated ODW consisted of a bow shock, a C-J ODW, a transverse detonation or shock wave that propagated in the

shock-compressed mixture by the bow shock, and an incident shock that propagated in the burned gas and made the Mach intersection. Though the observed SIC region became longer as the nondimensional projectile velocity was increased, the wave structure was fundamentally unchanged. The critical nondimensional projectile diameters to stabilize the ODW were about 3.5 for the $2C_2H_2 + 5O_2 + 7Ar$ mixture and 6.0 for the $2C_2H_2 + 5O_2 + 21Kr$ mixture. These experimental results indicate the possibility that the criticalities can't be expressed by only the ratio of the projectile diameter and the mixture cell size, but may also rely on the characterization of the mixture cellular structure.

S. Maeda, J. Kasahara, and A. Matsuo,
Combustion and Flame, Vol. 159 (2012) pp. 887-896.

Acknowledgements

I express my appreciation to Mr. Ryuichi Inada, Department of Engineering Mechanics and Energy, University of Tsukuba, for his help in performing these experiments.

This work was subsidized by the Ministry of Education, Culture, Sports, Science and Technology via a Grant-in-Aid for Scientific Research (A), No. 20241040; a Grant-in-Aid for Scientific Research (B), No. 21360411; and the Research Grant Program from the Institute of Space and Astronautical Science, the Japan Aerospace Exploration Agency.

S. Maeda, J. Kasahara, and A. Matsuo,
Combustion and Flame, Vol. 159 (2012) pp. 887-896.

References

[1] J.M. Powers, in: J. Buckmaster, T.L. Jackson, A. Kumar (Eds.), Combustion in High-Speed Flows, Kluwer Academic Publishers, Boston, 1994, pp. 345-371.

[2] A. Hertzberg, A. P. Bruckner, D. W. Bogdanoff, AIAA J. 26 (2) (1998) 195-203.

[3] A. J. Higgins, J. Propul. Power 22 (6) (2006) 1170-1187.

[4] H. F. Lehr, Astronautica Acta 17 (1972) 589-597.

[5] J. H. S. Lee, Prog. Astronaut. Aeronaut. 173 (1997) 293-310.

[6] A. A. Vasiljev, Shock Waves 3 (1994) 321-326.

[7] A. J. Higgins, A. P. Bruckner, AIAA paper 96-0342.

[8] M. J. Kaneshige, J. E. Shepherd, Proc. Combusti. Inst. 26 (1996) 3015-3022.

[9] J. Verreault, A. J. Higgins, Proc. Combusti. Inst. 33 (2011) 2311-2318.

[10] J. Kasahara, T. Horii, T. Endo, T. Fujiwara, Proc. Combusti. Inst. 26 (1996) 2903-2908.

[11] J. Kasahara, T. Fujiwara, T. Endo, T. Arai, AIAA J. 39 (8) (2001) 1553-1561.

[12] J. Kasahara, T. Arai, S. Chiba, K. Takazawa, Y. Tanahashi, A. Matsuo, Proc. Combusti. Inst. 29 (2002) 2817-2824.

[13] S. Yu. Chernyavskii, N. N. Baulin, A. S. Mkrtumov, Combustion, Explosion, and Shock Waves 9 (1973) 687-690.

[14] S. Maeda, R. Inada, J. Kasahara, A. Matsuo, Proc. Combusti. Inst. 33 (2011) 2343-2349.

[15] D. Desbordes, Prog. Astronaut. Aeronaut. 114 (1988) 170-185.

[16] D. Desbordes, C. Guerraud, L. Hamada, H. N. Presles, Prog. Astronaut. Aeronaut. 153 (1993) 347-359.

[17] M. J. Kaneshige, J. E. Shepherd, Detonation Database, Technical Report No. FM97-8, GALCIT, Pasadena, CA, 1997.

[18] W. C. Reynolds, The Element Potential Method for Chemical Equilibrium Analysis: Implementation in the Interactive Program STANJAN: Version 3, Technical Report No. A-3991, Stanford Univ., 1986.

[19] C. Li, K. Kailasanath and S. Oran, Phys. Fluids 6 (1994) 1600-1611.

[20] A. Matsuo and K. Fujii, AIAA Journal 33 (1995) 1828-1835.

[21] H. Behrens, W. Struth and F. Wecken, Symposium (International) on Combustion 10 (1965) 245-252.

[22] M. I. Radulescu, A. J. Higgins, S. B. Murray, J. H. S. Lee, J. Fluid Mech. 480 (2003) 1-24.

[23] J. H. S. Lee, The Detonation Phenomenon, Cambridge University Press, New York, 2008.

S. Maeda, J. Kasahara, and A. Matsuo,
Combustion and Flame, Vol. 159 (2012) pp. 887-896.

Table 1
The experimental conditions.

V_p / D_{CJ} condition	Mixture	Filling pressure	V_p / D_{CJ}	d / λ	Result	Figure
-	-	±0.05 kPa	±0.65 %	±0.5 %	-	-
Low	$2C_2H_2+5O_2+7Ar$	26.2	1.22	2.98	×	Fig. 2 (d)
		28.8	1.28	3.30	△	Fig. 2 (c)
		31.4	1.19	3.63	○	Fig. 2 (b)
		41.2	1.21	4.92	●	Fig. 2 (a)
Low	$2C_2H_2+5O_2+21Kr$	61.4	1.05	4.93	×	Fig. 2 (h)
		70.3	1.11	5.81	△	Fig. 2 (g)
		72.9	1.10	6.07	○	Fig. 2 (f)
		81.1	1.09	6.90	●	Fig. 2 (e)
Medium	$2C_2H_2+5O_2+21Kr$	70.0	1.50	5.77	△	Fig. 8 (c), (c')
		72.0	1.48	5.97	●	Fig. 8 (b)
		75.4	1.53	6.32	●	Fig. 8 (a)
High	$2C_2H_2+5O_2+21Kr$	62.2	1.78	5.01	×	
		71.2	1.68	5.89	△	
		71.9	1.79	5.96	□	Fig. 12
		74.7	1.66	6.25	●	Fig. 8 (e)
		82.1	1.64	7.00	●	Fig. 8 (d)

Filling temperatures were 278.3～303.6 ± 2.5 K (room temperatures).
×: Shock-induced combustion, △: Straw Hat type with an attenuated ODW, □: Shock-induced combustion and spherical detonations, ○: Straw Hat type with a stabilized ODW, and ●: Stabilized ODW.

Table 2
The horizontal traveling velocities of the transition points for a Straw Hat type with an attenuated ODW.

Mixture	V_p / D_{CJ}	V_p	V_{tr}	D_{CJ}
-	±0.65 %	±20 m/s	±20 m/s	m/s
$2C_2H_2+5O_2+7Ar$	1.09	2130	2010	1955
$2C_2H_2+5O_2+7Ar$	1.28	2510	2020	
$2C_2H_2+5O_2+21Kr$	1.11	1410	1350	1275

S. Maeda, J. Kasahara, and A. Matsuo,
Combustion and Flame, Vol. 159 (2012) pp. 887-896.

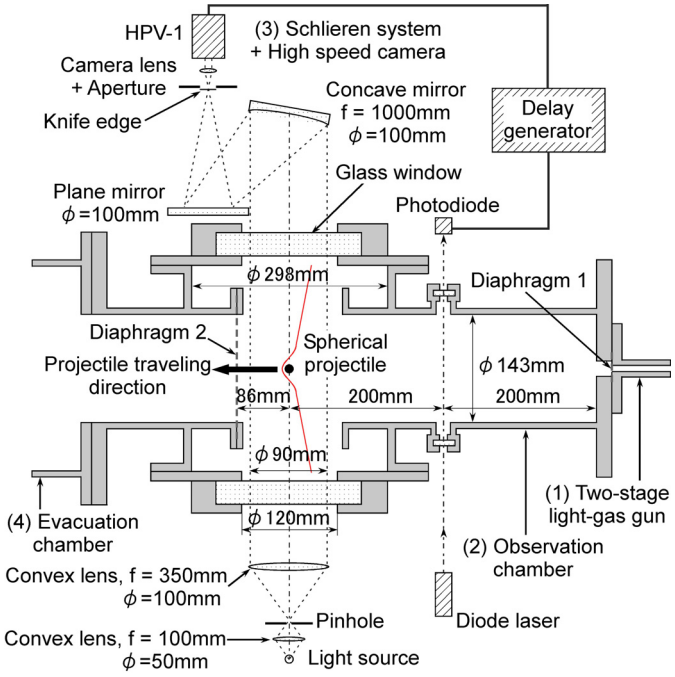

Fig. 1. A schematic diagram of the experimental arrangement (top view).

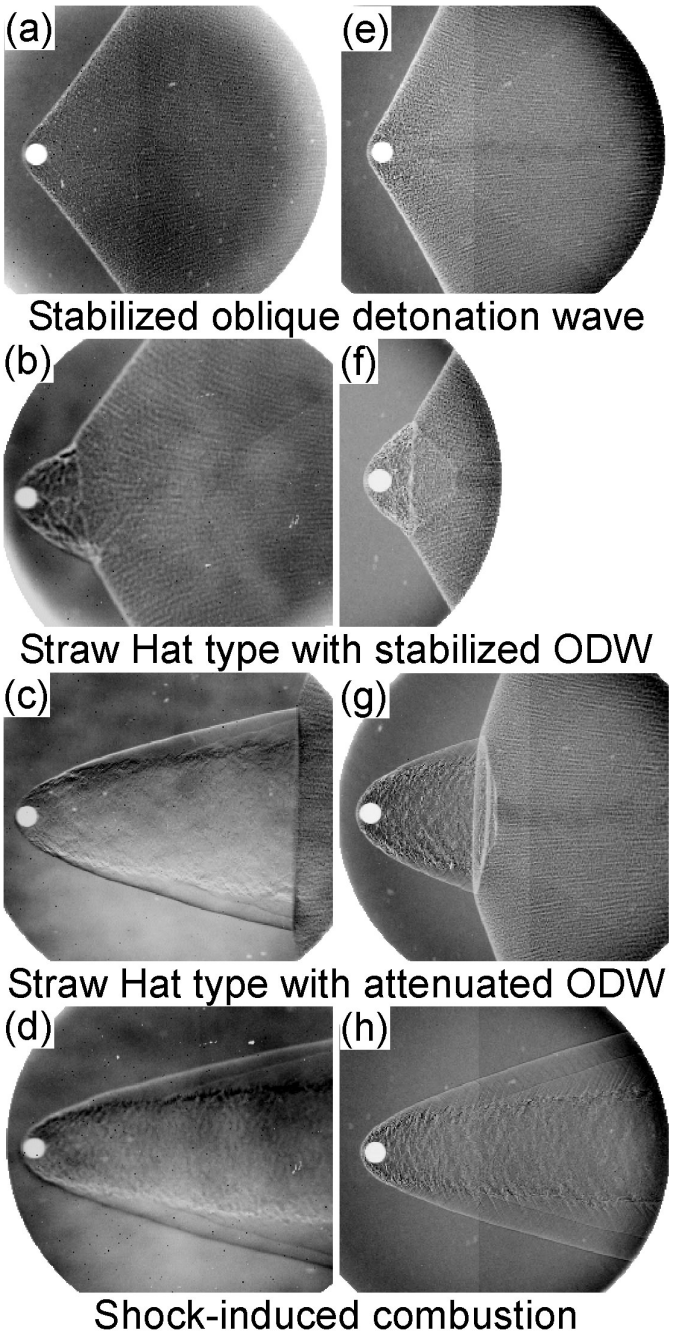

Fig. 2. Snapshots of the movies under low V_p / D_{CJ} conditions (negative pictures).

(a)～(d): $2C_2H_2+5O_2+7Ar$, V_p / D_{CJ} = 1.24±0.04

(e)～(h): $2C_2H_2+5O_2+21Kr$, V_p / D_{CJ} = 1.08±0.03

(a) p_0 = 41.2kPa, d/λ = 4.92, (b) p_0 = 31.4kPa, d/λ = 3.63

(c) p_0 = 28.8kPa, d/λ = 3.30, (d) p_0 = 26.2kPa, d/λ = 2.98

(e) p_0 = 81.1kPa, d/λ = 6.90, (f) p_0 = 72.9kPa, d/λ = 6.07

(g) p_0 = 70.3kPa, d/λ = 5.81, (h) p_0 = 61.4kPa, d/λ = 4.93

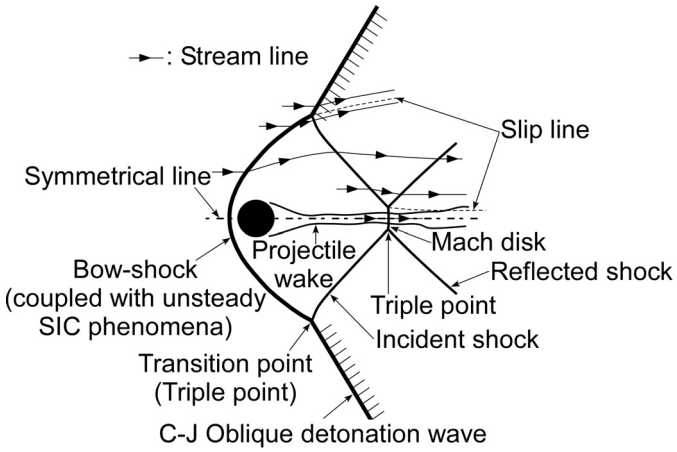

Fig. 3. The wave structure of the Straw Hat type with a stabilized ODW (a central cross section of the axisymmetric phenomenon).

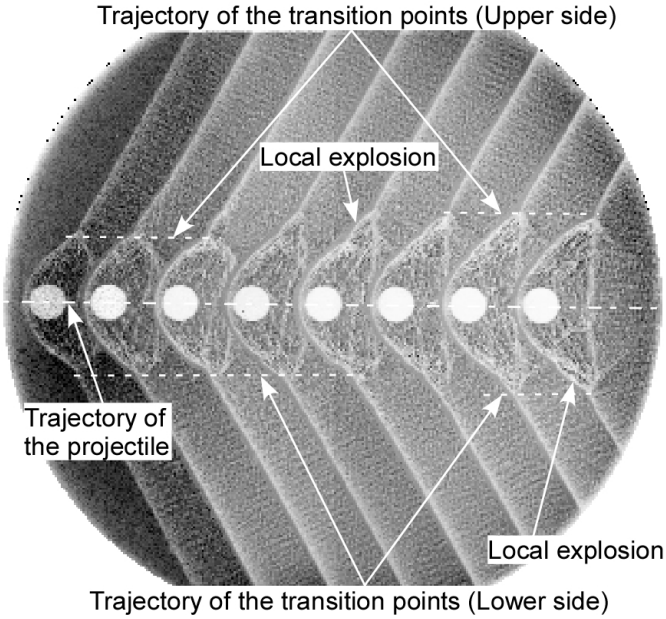

Fig. 4. A superposed picture (7-μs intervals) of the movie of a Straw Hat type with a stabilized ODW, which corresponds to Fig. 2 (f) (negative picture).

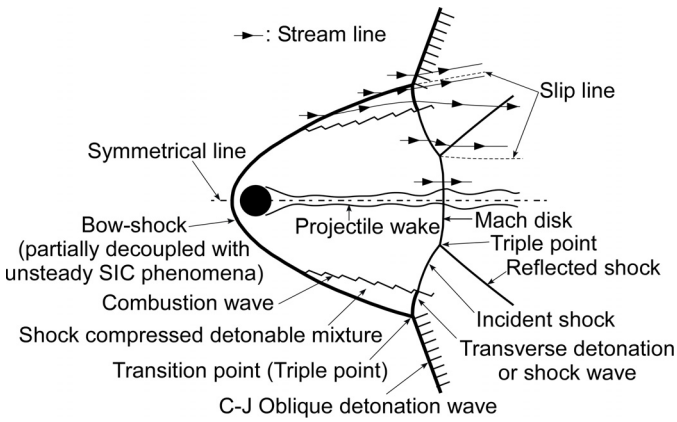

Fig. 5. The wave structure of the Straw Hat type with an attenuated ODW (a central cross section of the axisymmetric phenomenon).

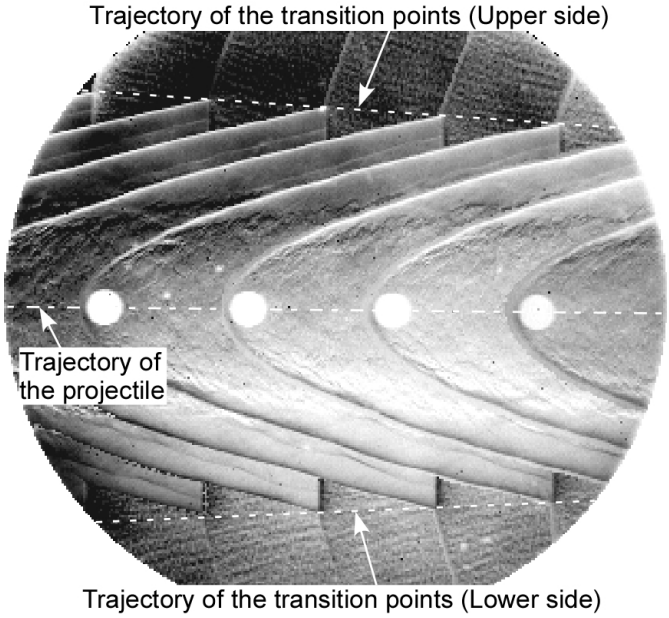

Fig. 6. A superposed picture (8-μs intervals) of the movie of a Straw Hat type with an attenuated ODW, which corresponds to Fig. 2 (c) (negative picture).

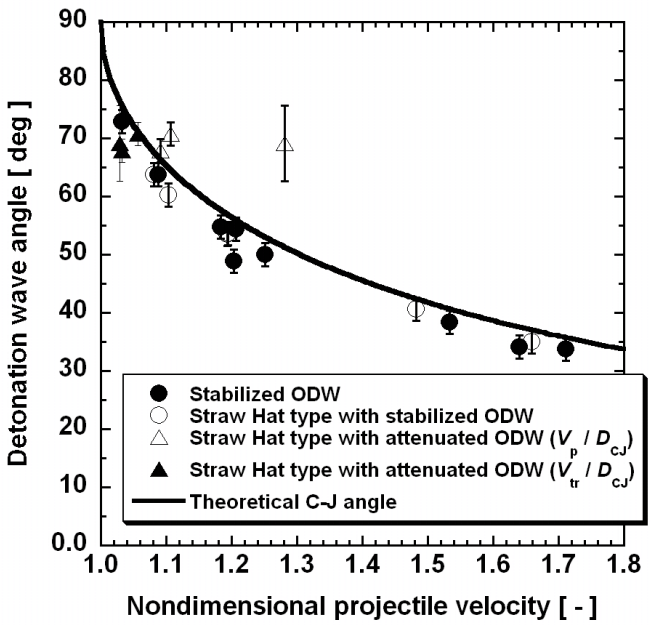

Fig. 7. The relationship between the nondimensional projectile velocity and the detonation wave angle.

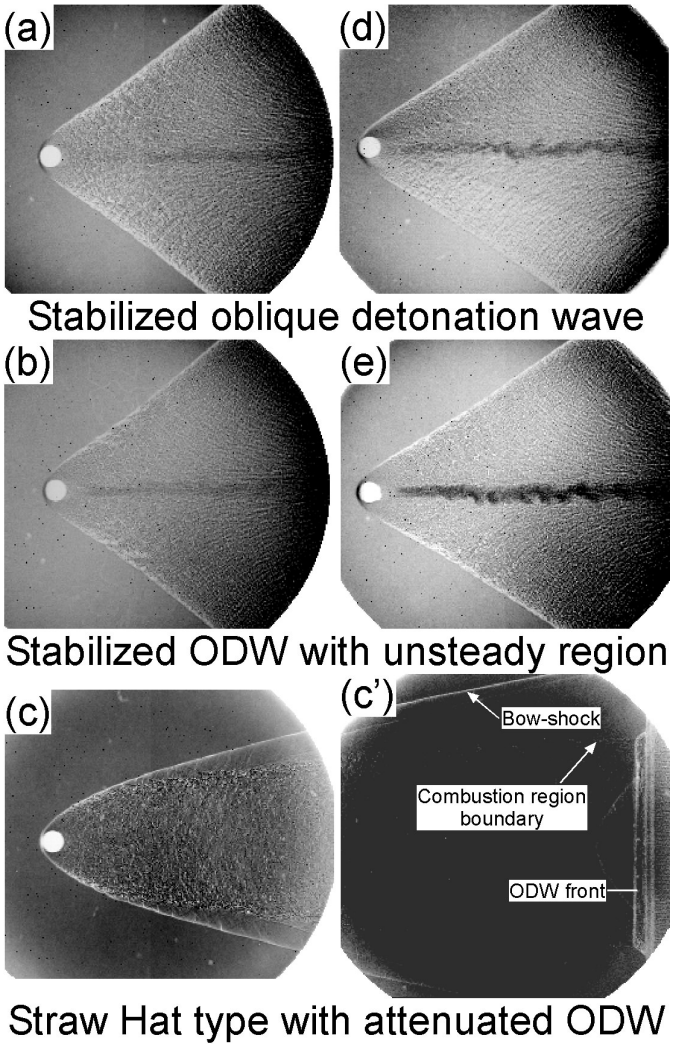

Fig. 8. Snapshots of the movies under the medium and high V_p / D_{CJ} conditions (negative pictures).

(a)～(c), (c'): medium V_p / D_{CJ} condition

(d), (e): high V_p / D_{CJ} condition

(a) p_0 = 75.4kPa, d/λ = 6.32, (b) p_0 = 72.0kPa, d/λ = 5.97

(c), (c') p_0 = 70.0kPa, d/λ = 5.77

(d) p_0 = 82.1kPa, d/λ = 7.00, (e) p_0 = 74.7kPa, d/λ = 6.25

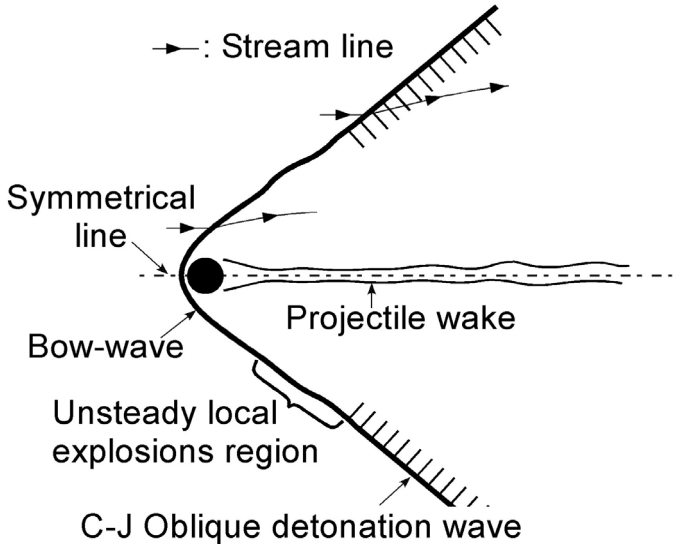

Fig. 9. The wave structure of the stabilized ODW with an unsteady region under the medium and high V_p / D_{CJ} conditions (a central cross section of the axisymmetric phenomenon).

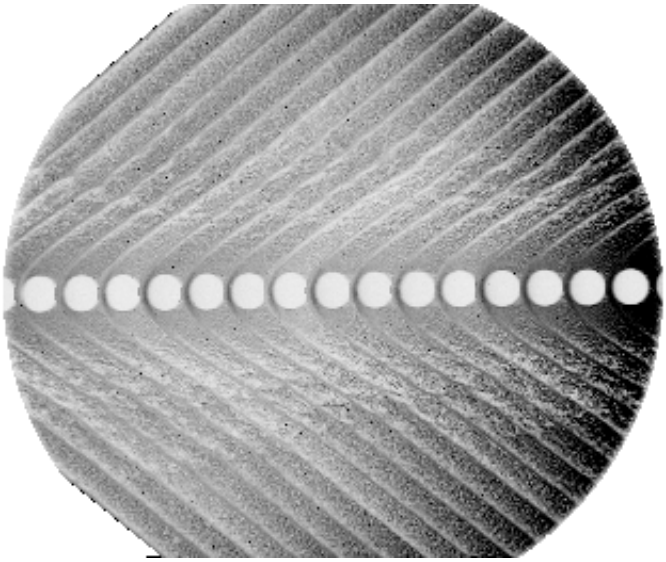

Fig. 10. A superposed picture (3-μs intervals) of the movie of a stabilized ODW with an unsteady region, which corresponds to Fig. 8 (b) (negative picture).

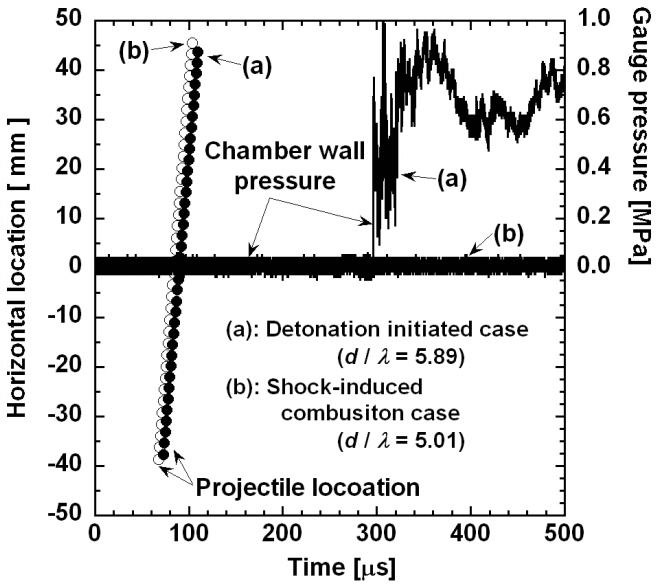

Fig. 11. Time histories of the projectile locations and the chamber wall pressures for $d / \lambda = 5.01$ and 5.89, the high V_p / D_{CJ} conditions.

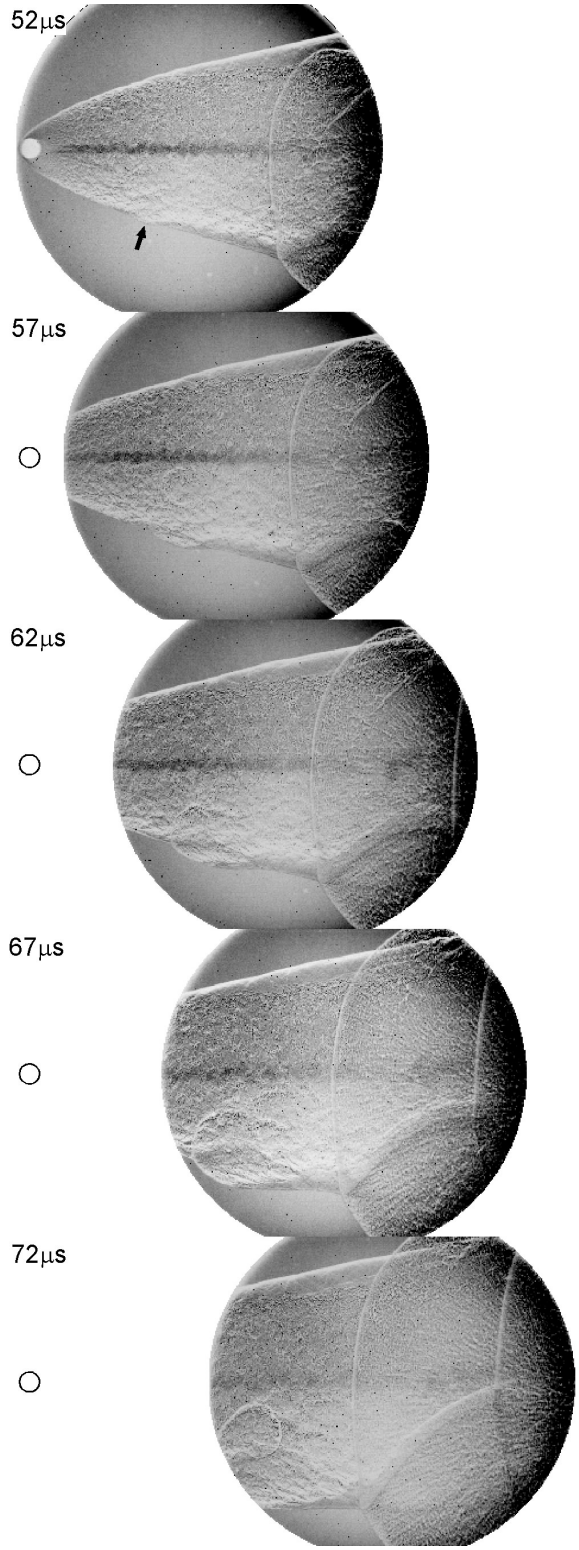

Fig. 12. Continuous pictures of a shock-induced combustion and spherical detonations.

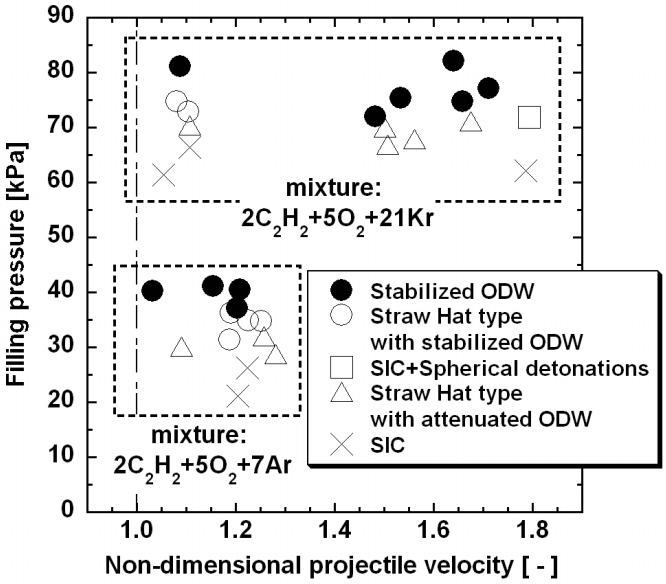

Fig. 13. The observed phenomena at various nondimensional projectile velocities and filling pressures.

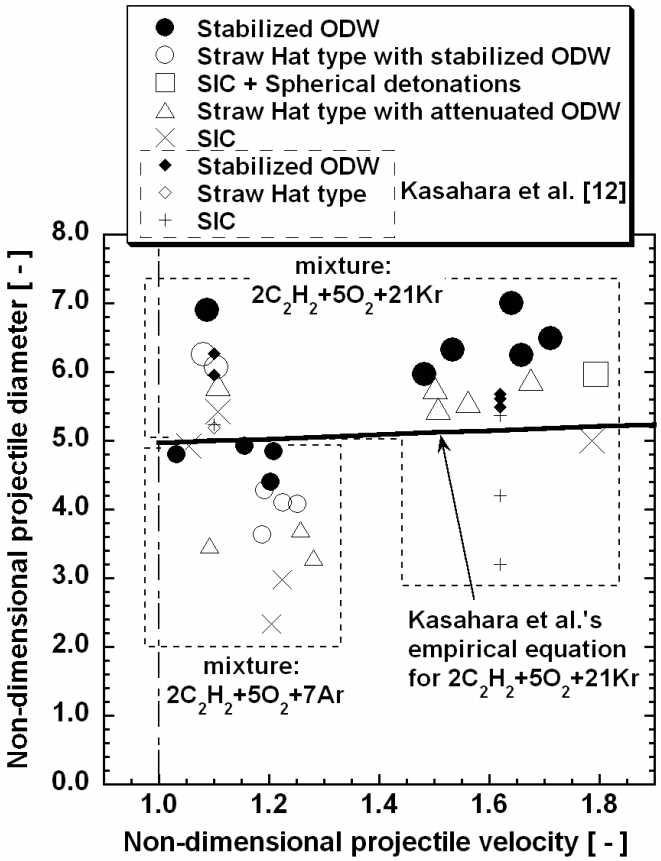

Fig. 14. The observed phenomena at various nondimensional projectile velocities and diameters using the $2C_2H_2+5O_2+7Ar$ mixture and $2C_2H_2+5O_2+21Kr$ mixture. The results of previous work using the $2C_2H_2+5O_2+21Kr$ mixture refer to Kasahara *et al.* [12].